# Supporting Information

# Electrodeposited dual-phase nickel selenide heterostructure for hydrazine-assisted water splitting

Amit Kumar Nayak, Gaurav Mehta, and Debabrata Pradhan*

*Materials Science Centre, Indian Institute of Technology Kharagpur, West Bengal 721 302, India*

**Table S1.** List of samples obtained by varying operating potentials while maintaining a constant electrodeposition duration of 1 h.

| Precursor | Time | Potential | Deposited Product | Synthesized electrode |
|---|---|---|---|---|
| $NiCl_2.6H_2O$ $SeO_2$ LiCl Water + Ni foam | 60 min | –0.45 V | $NiSe_2$ | $NiSe_2$@NF |
| | | –0.5 V | $NiSe_2/Ni_{0.85}Se$ | NSNS-1@NF |
| | | –0.55 V | $NiSe_2/Ni_{0.85}Se$ | NSNS-2@NF **(NSNS@NF)** |
| | | –0.6 V | $NiSe_2/Ni_{0.85}Se$ | NSNS-3@NF |
| | | –0.65 V | $Ni_{0.85}Se$ | $Ni_{0.85}Se$@NF |

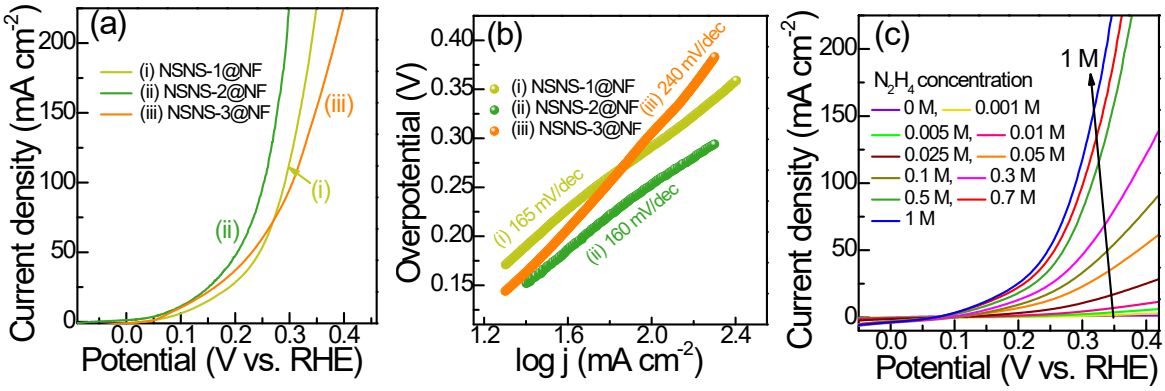


**Figure S1.** (a) Electrocatalytic HzOR activities of (i) NSNS-1@NF, (ii) NSNS-2@NF, and (iii) NSNS-3@NF in 1.0 M KOH + 0.5 M $N_2H_4$. The polarization curves were obtained at a scan rate of 5 mV $s^{-1}$. (b) Corresponding Tafel plots. (c) Electrocatalytic HzOR by varying $N_2H_4$ concentrations in 1.0 M KOH with NSNS-2@NF or NSNS@NF.

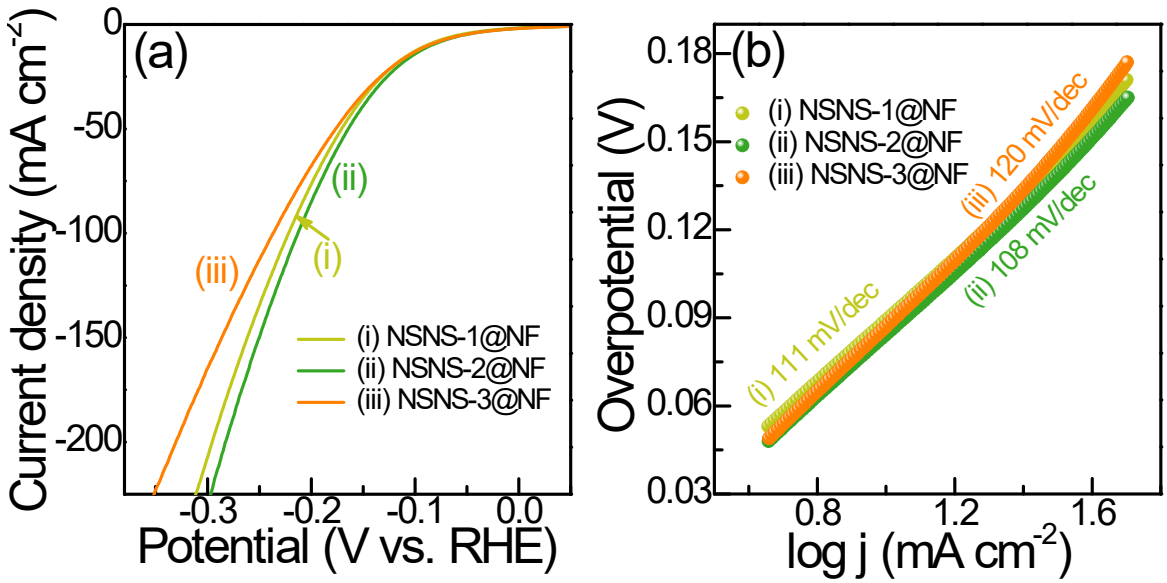


**Figure S2.** (a) Electrocatalytic HER activities of (i) NSNS-1@NF, (ii) NSNS-2@NF, and (iii) NSNS-3@NF in 1.0 M KOH + 0.5 M $N_2H_4$. The polarization curves were collected at a scan rate of 5 mV $s^{-1}$. (b) Corresponding Tafel plots.

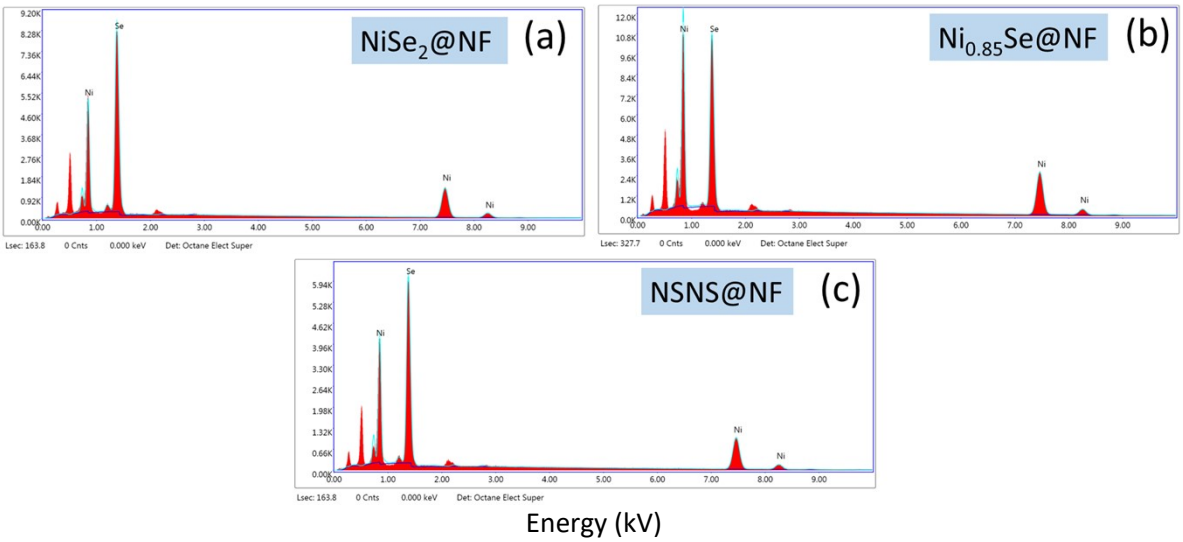


**Figure S3.** EDX spectra of (a) $NiSe_2$@NF, (b) $Ni_{0.85}Se$@NF, and (c) NSNS@NF.

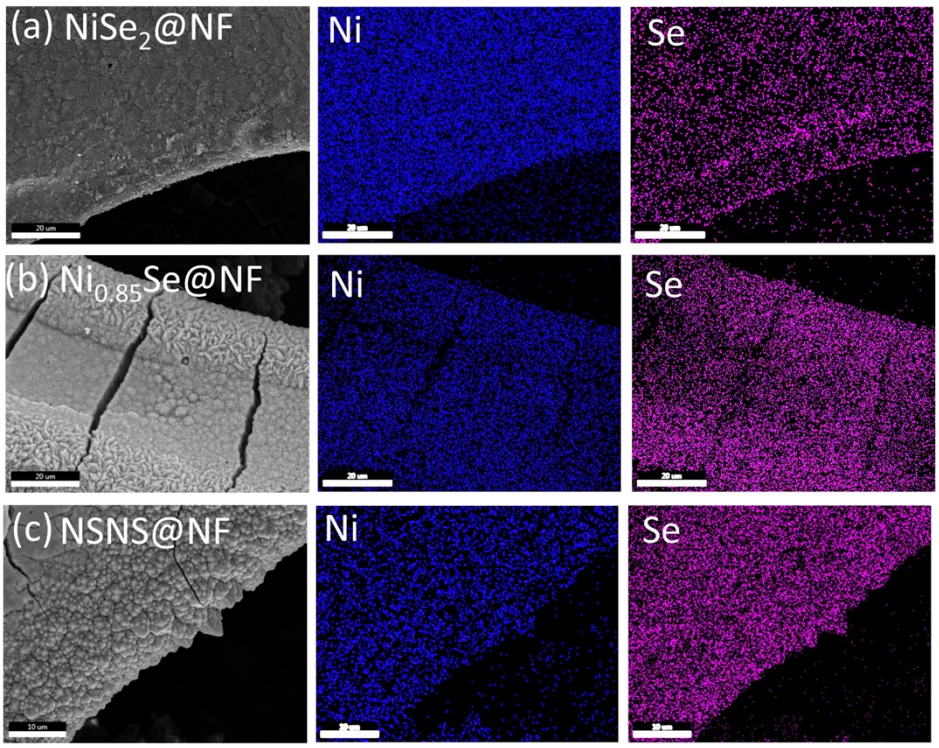


**Figure S4.** FESEM image and corresponding EDX elemental mapping of (a) $NiSe_2$@NF, (b) $Ni_{0.85}Se$@NF, and (c) NSNS@NF, confirming the uniform distribution of Ni and Se.

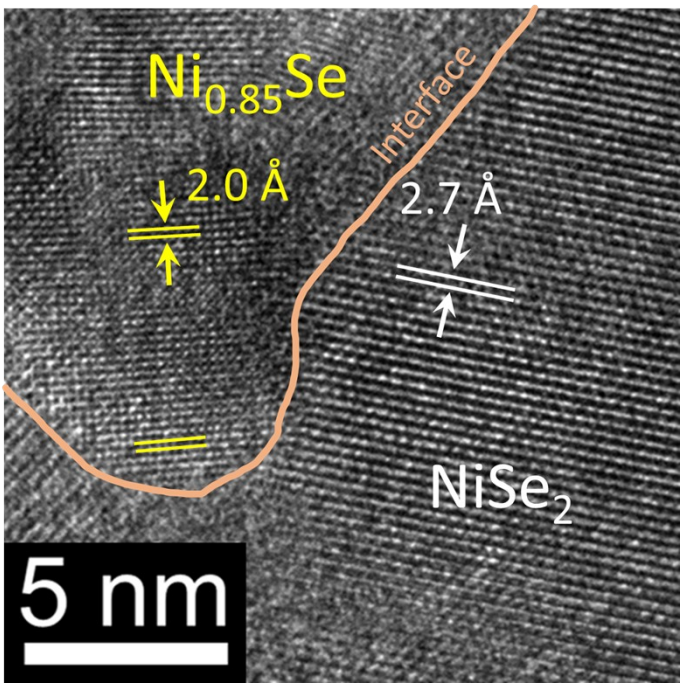


**Figure S5.** HRTEM image depicting the $NiSe_2/Ni_{0.85}Se$ heterointerface.

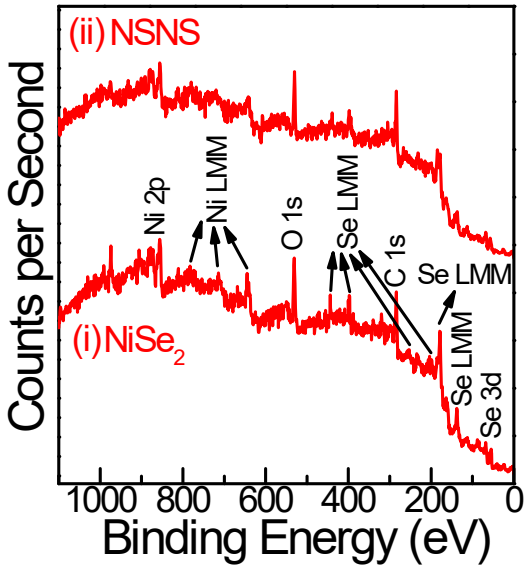


**Figure S6.** Survey XPS spectrum of (i) $NiSe_2$ and (ii) NSNS heterostructure.

**Table S2.** Comparison of HzOR activity of NSNS@NF with the recently reported non-noble catalysts.

| *Electrocatalyst* | *HzOR potential (mV@10 mA cm$^{-2}$)* | *Reference* |
|---|---|---|
| NSNS@NF | 94 | This work |
| Ru–$VO_x$/$Ni_3S_2$ | –66 | 1 |
| $Ni(OH)_2$/$Ni_2P$/NF | –14 | 2 |
| Al-$Ni_2P$/NF | 5 | 3 |
| $Ni_{1.4}Mn_{0.6}P$ NCs | 55 | 4 |
| Fe/P-$NiMoO_4$ | 90 | 5 |
| $Rh_2S_3$/NC | 95 | 6 |
| $Co_{0.5}$NiS-NSs/NF | 110 | 7 |
| $(Ni,Co)_{0.85}Se$/rGO | 124 | 8 |
| $Co_9S_8$/$CoTe_2$ | 125 | 9 |
| Mn-SA/BNC | 132 | 10 |
| Co-$MoS_2$/$V_2C$@CC | 170 | 11 |
| Cu-CoFe/Co/NC | 281 | 12 |

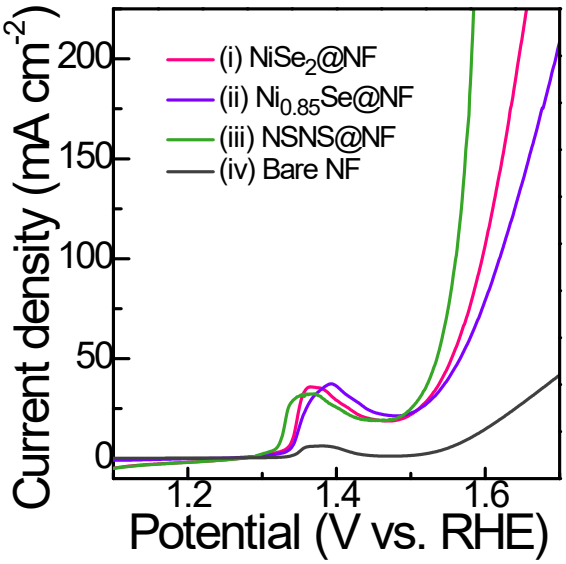


**Figure S7.** LSV curves of $NiSe_2$@NF, $Ni_{0.85}Se$@NF, NSNS@NF, and bare NF for electrocatalytic OER activity in 1.0 M KOH.

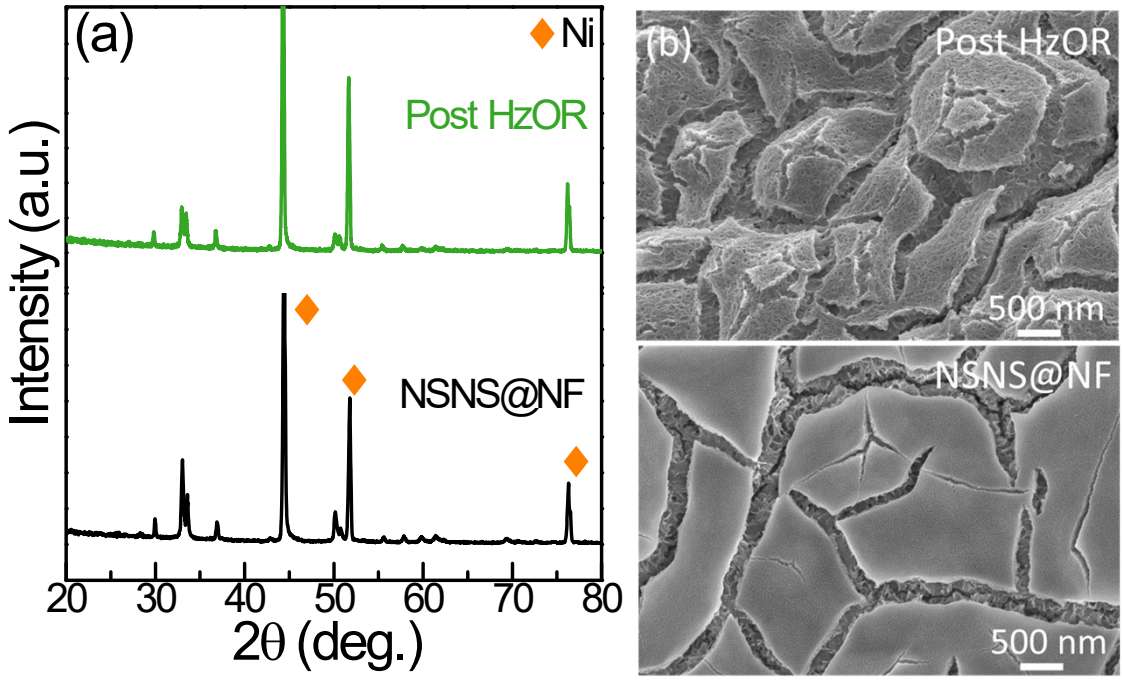


**Figure S8.** (a) XRD patterns and (b) FESEM images of NSNS@NF before and after 48 h HzOR, and (c) elemental mapping of NSNS@NF after 48 h HzOR in 1.0 M KOH + 0.5 M $N_2H_4$.

**Roughness factor calculation**

First, the electrochemically active surface area (ECSA) was determined before and after 48 h of continuous operation, from the double-layer capacitance measurements obtained in a non-Faradaic potential region. The surface roughness factor ($R_f$) was then calculated as the ratio of ECSA to the electrode's geometric surface area (1 $cm^2$).

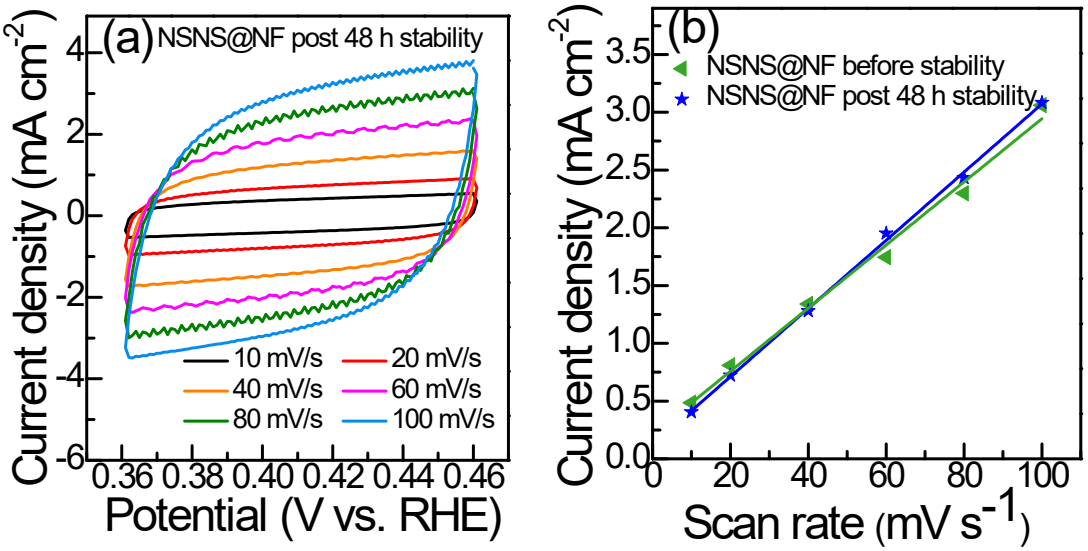


**Figure S9.** (a) CV curves of NSNS@NF after 48 h HzOR stability test at different scan rates. (b) The double-layer capacitive current of NSNS@NF before and after stability test at 0.41 V (versus RHE) as a function of scan rate.

**Table S3**. ECSA and roughness factor calculation for NSNS@NF electrode before and after the 48 h HzOR stability test.

| *Sample* | $C_{dl}$ *(mF cm$^{-2}$)* | *ECSA (cm$^2$)* | $R_f$ |
|---|---|---|---|
| NSNS@NF before stability test | 27.3 | 682.5 | 682.5 |
| NSNS@NF post 48h stability test | 29.5 | 737.5 | 737.5 |

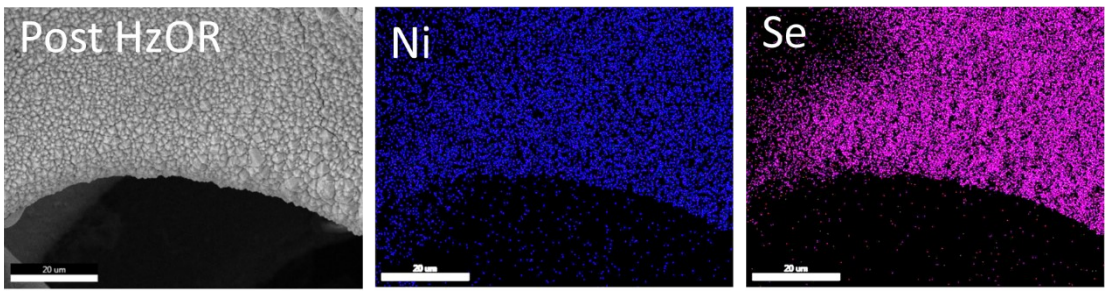


**Figure S10.** Elemental mapping of NSNS@NF after 48 h HzOR in 1.0 M KOH + 0.5 M $N_2H_4$.

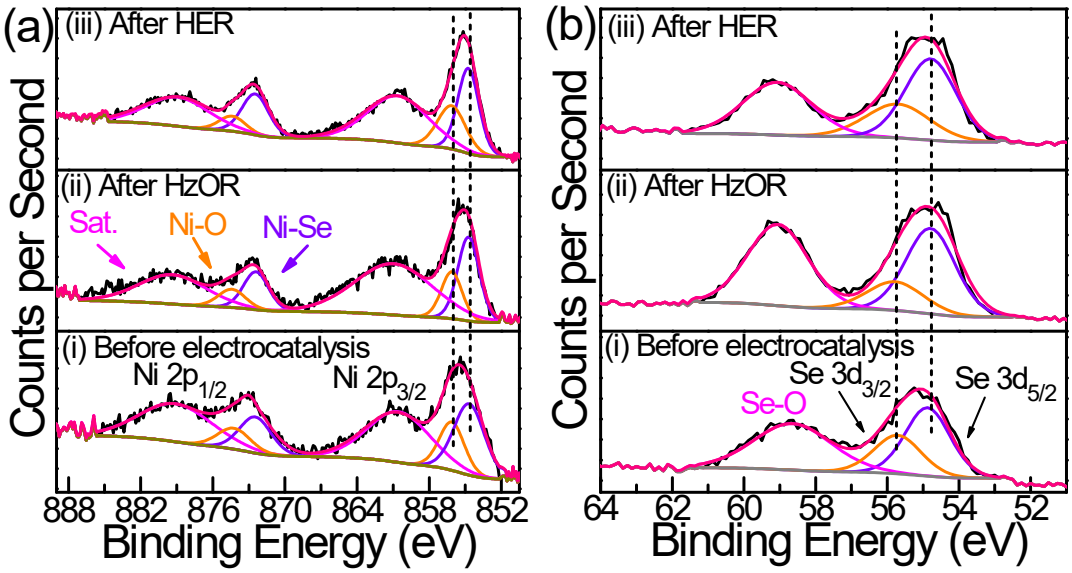


**Figure S11.** High-resolution (a) Ni 2p and (b) Se 3d XPS spectra of NSNS heterostructure (i) before electrocatalysis, (ii) after HzOR, and (iii) after HER activity for 48 h.

**Table S4.** Comparison of HER activity of NSNS@NF with the recently reported non-noble catalysts.

| *Electrocatalyst* | *HER overpotential (mV@10 mA cm$^{-2}$)* | *Reference* |
|---|---|---|
| NSNS@NF | 85 | This work |
| Pt-Ru/$RuO_2$ | 18 | [13] |
| Ru@$MoS_2$/CFP | 19 | [14] |
| $Ru_2P$/$Ir_2P$ HNT | 23 | [15] |
| NiFeS@NiMoP/NF | 56 | [16] |
| POM-$Fe_{0.2}Ni_{0.8}Co_2O_4$/NF | 89 | [17] |
| $MoSe_2$@NiSe NW | 105 | [18] |
| $MoS_{1.34}Se_{0.78}$ | 108 | [19] |
| NiFeHCF@NF | 125 | [20] |
| NiSA-O/$Mo_2C$ | 133 | [21] |
| CoTe/$CoNiSe_2$ | 140 | [22] |
| $Co_2$-NiSe/NF | 149 | [23] |
| NMS/NF | 181 | [24] |

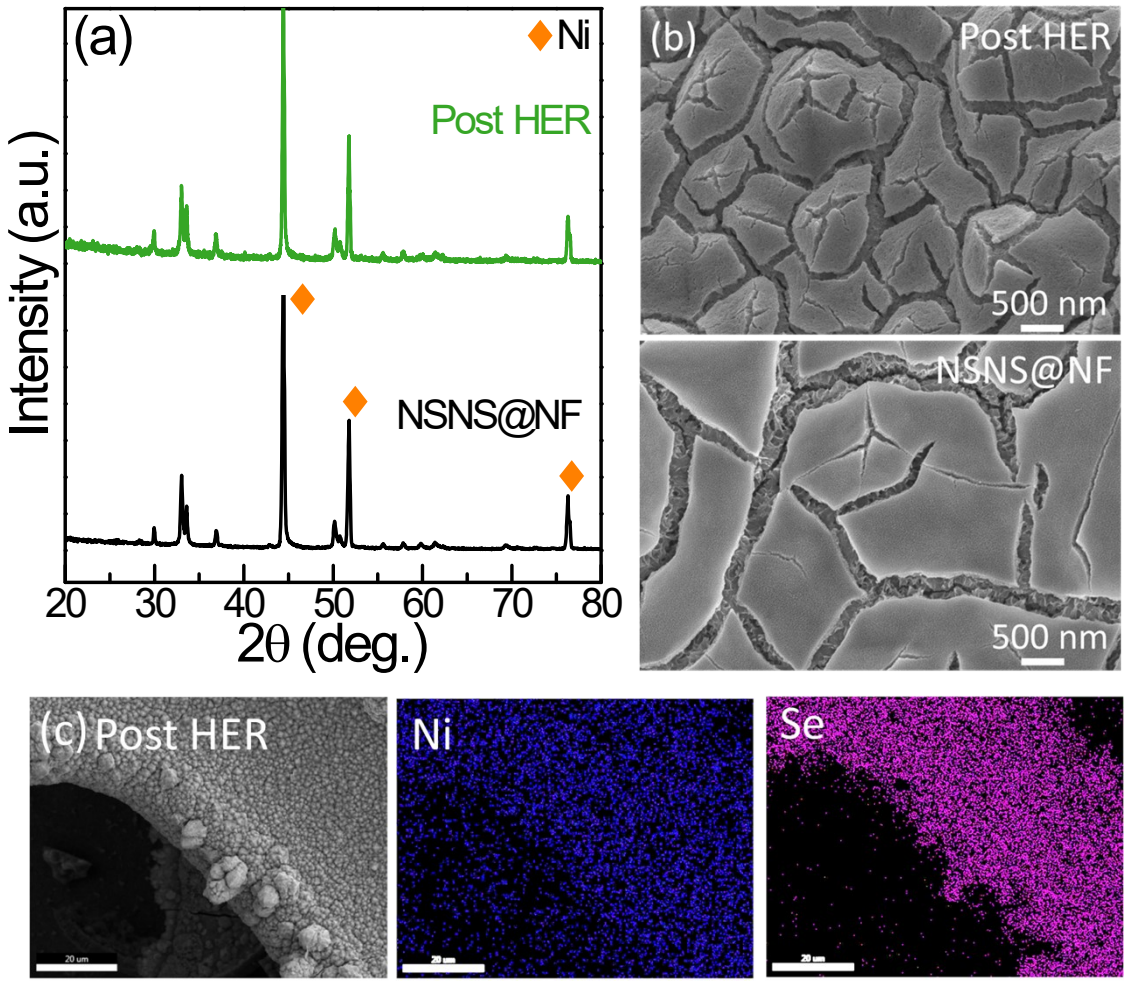


**Figure S12.** (a) XRD patterns and (b) FESEM images of NSNS@NF before and after 48 h HER, and (c) elemental mapping of NSNS@NF after 48 h HER in 1.0 M KOH.

**Table S5.** Mass activity value of the samples.

| | *Mass activity (A $g^{-1}$)* | |
|---|---|---|
| *Catalyst* | *At a HER potential of –0.2 V* | *At a HzOR potential of +0.2 V* |
| $NiSe_2$@NF | 76.3 | 25.1 |
| $Ni_{0.85}Se$@NF | 97.7 | 43.5 |
| NSNS@NF | 125.0 | 69.8 |
| State-of-the-art catalyst | 378.2 (for Pt/C@NF) | 58.2 (for $IrO_2$@NF) |

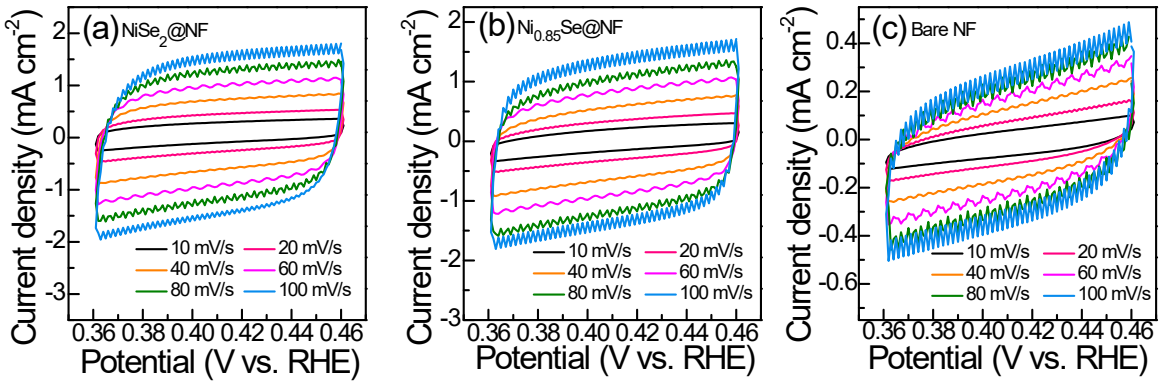


**Figure S13.** CV curves measured at different scan rates from 10 to 100 mV $s^{-1}$ and at a potential range of 0.36 V to 0.46 V (vs. RHE) of (a) $NiSe_2$@NF, (b) $Ni_{0.85}Se$@NF, and (c) bare NF.

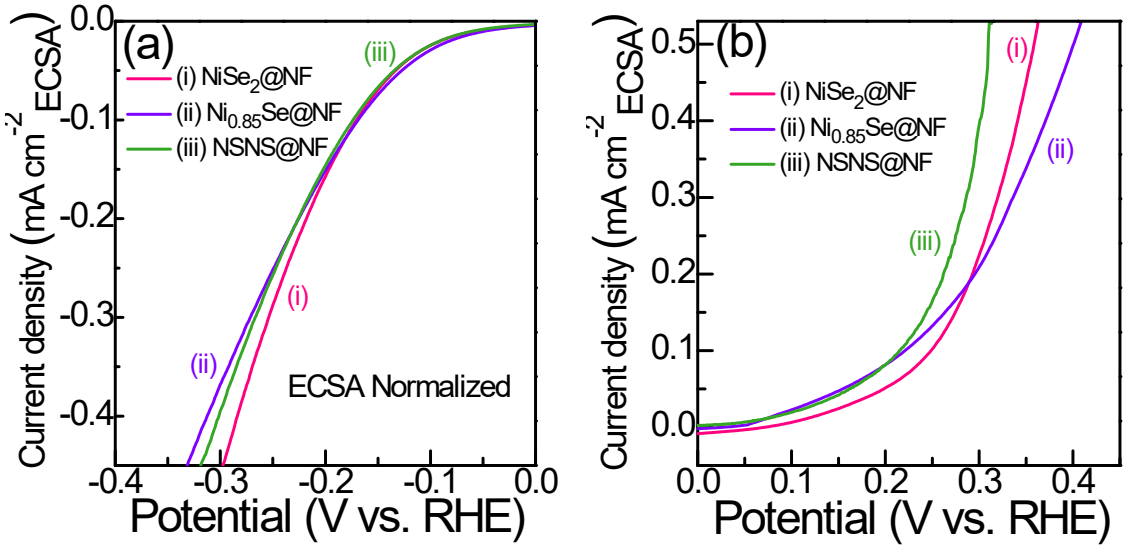


**Fig. S14**. ECSA normalized (a) HER and (b) HzOR polarization curves of the as-prepared $NiSe_2$@NF and $Ni_{0.85}Se$@NF, and NSNS@NF.

**Table S6.** Comparison of OHzS performance of NSNS@NF with the recently reported non-noble catalysts.

| *Electrocatalyst* | *OHzS Cell voltage (V@10 mA cm$^{-2}$)* | *Reference* |
|---|---|---|
| NSNS@NF | 0.11 | This work |
| Ru-(Ni/Fe)$C_2O_4$ | 0.01 | 25 |
| Ru–$VO_x$/$Ni_3S_2$ | 0.015 | 1 |
| $CoFe_2O_4$@NNWs | 0.028 | 26 |
| Al-$Ni_2P$/NF | 0.068 | 3 |
| $V_{Se}$-$CoSe_2$/$MoSe_2$ | 0.108 | 27 |
| $Ru_{SA}$/v-$Mo_2C$ | 0.12 | 28 |
| Ir/CoP | 0.125 | 29 |
| Fe/P-$NiMoO_4$ | 0.13 | 5 |
| Co(OH)F/Co−S/$CeO_2$/NF | 0.2 | 30 |
| Co−FeNiSOH/NFF | 0.26 | 31 |
| Cu-CoFe/Co/NC | 0.66 | 12 |

**Faradaic efficiency calculation**

The Faradaic efficiency was determined by comparing the volume of gas measured experimentally (at a current density of 500 mA cm$^{-2}$ over a 200 s period) with the theoretical volume of gas. Assuming that two electrons are used to produce one $H_2$ molecule, the Faradaic efficiency for $H_2$ production can be calculated by the following equation S1.

$$FE\ (H_2) = \left(\frac{V_{experimental}}{V_{theoritical}}\right) \times 100\% \quad \text{(S1)}$$

The theoretical volume of the gas can be determined using Faraday's law, as shown in equation S2.

$$V_{theoritical} = \frac{I \times t \times V_m}{n \times F} \quad \text{(S2)}$$

where $I$ represents the current in amperes, $t$ represents the recorded time in seconds, $V_m$ indicates the molar volume of $H_2$ in L mol$^{-1}$, $n$ is the number of moles of electrons required to produce 1 mol of $H_2$, and F denotes the Faraday constant (96485 C mol$^{-1}$).

## References


[1] Z. Liu, Y. Li, H. Guo, J. Zhao, H. Zhang and R. Song, *J. Mater. Chem. A*, 2023, **11**, 24667-24677.

[2] H.-M. Yang, H.-Y. Wang, M.-L. Sun and Z.-Y. Yuan, *Chem. Eng. J.*, 2023, **475**, 146134.

[3] H.-M. Yang, H.-Y. Wang, S. Zhai, J.-T. Ren and Z.-Y. Yuan, *Chem. Eng. J.*, 2024, **489**, 151236.

[4] U. P. Suryawanshi, U. V. Ghorpade, P. V. Kumar, J. S. Jang, M. He, H. J. Shim, H. R. Jung, M. P. Suryawanshi and J. H. Kim, *Appl. Catal. B: Environ.*, 2024, **355**, 124165.

[5] Z. Zhao, Z. Li, Z. Zhang and X. Meng, *Appl. Catal. B: Environ.*, 2024, **347**, 123805.

[6] C. Zhang, H. Liu, Y. Liu, X. Liu, Y. Mi, R. Guo, J. Sun, H. Bao, J. He, Y. Qiu and J. Ren, *Small Methods*, 2020, **4**, 2000208.

[7] X.-H. Wang, R. Yuan, S.-B. Yin, Q.-L. Hong, Q.-G. Zhai, Y.-C. Jiang, Y. Chen and S.-N. Li, *Adv. Funct. Mater.* 2024, **34**, 2310288.

[8] Z. Feng, T. Shi, W. Liu, W. Zhang and H. Zhang, *Int. J. Energy Res.* 2022, **46**, 15938–15947.

[9] V. Mishra, A. E. Praveen, D. Raveendran, A. Chandrasekar and V. Mahalingam, *Small*, 2025, **21**, 2412372.

[10] X. Peng, J. Hou, Y. Mi, J. Sun, G. Qi, Y. Qin, S. Zhang, Y. Qiu, J. Luo and X. Liu, *Nanoscale*, 2021, **13**, 4767–4773.

[11] Y. Chen, G. Meng, T. Yang, C. Chen, Z. Chang, F. Kong, H. Tian, X. Cui, X. Hou and J. Shi, *Chem. Eng. J.*, 2022, **450**, 138157.

[12] X. Liu, H. Mao, G. Liu, Q. Yu, S. Wu, B. Li, G. Zhou, Z. Li and L. Wang, *Chem. Eng. J.*, 2023, **451**, 138699.

[13] Y. Zhu, M. Klingenhof, C. Gao, T. Koketsu, G. Weiser, Y. Pi, S. Liu, L. Sui, J. Hou, J. Li and H. Jiang, *Nat. Commun.*, 2024, **15**, 1447.

[14] C. Xu, H. Yu, H. Huang, W. Huang, S. Li, Y. Cao, H. Lu, G. Li, Y. Li, X. Li and Y. Zhang, *Chem. Eng. J.*, 2024, **489**, 151295.

[15] Y. Hong, S. Jeong, J. H. Seol, T. Kim, S. C. Cho, T. K. Lee, C. Yang, H. Baik, H. S. Park, E. Lee and S. J. Yoo, *Adv. Energy Mater.*, 2024, **14**, 2401426.

[16] S. Yang, T. Wen and Y. Gong, *Int. J. Hydrogen Energy*, 2024, **68**, 834-842.

[17] L.-P. Cui, Y.-W. Wang, K. Yu, Y.-J. Ma and B.-B. Zhou, *Adv. Funct. Mater.* 2024, **34**, 2408968.

[18] J. Mao, W. Wang, J. Kang, K. Fang, Y. Shao and J. Yuan, *Int. J. Hydrogen Energy*, 2024, **78**, 1048–1059.

[19] Q. Zhou, Z. Liu, X. Luo, X. Qin and W. Xu, *Nanoscale*, 2025, **17**, 24272–24278.

[20] A. Gayathri, V. Ashok, M. Sangamithirai, J. Jayabharathi and V. Thanikachalam, *Green Chem.* 2024, **26**, 5326–5338.

[21] M. Hou, L. Zheng, D. Zhao, X. Tan, W. Feng, J. Fu, T. Wei, M. Cao, J. Zhang and C. Chen, *Nat. Commun.* **15**, 1342.

[22] D. Atallah, T. Ali Shah, G. Rodriguez-Ortiz, M. Nauman Ullah, F. Mahmood, G. A. Shazly and M. Waqas, *ACS Appl. Energy Mater.,* 2024, **7**, 10693–10700.

[23] J. Xu, J. Ruan, Y. Jian, J. Lao, Z. Li, F. Xie, Y. Jin, X. Yu, M.-H. Lee, Z. Wang and N. Wang, *Small*, 2024. **20**, 2305905.

[24] H. Sharan, A. Kausalya, S. Lakshmipathi, J. Madhavan, P. Karthikesan and A. Mani, *ACS Appl. Energy Mater.* 2025, **8**, 13752–13762.

[25] J. Zhao, H. Guo, Q. Zhang, Y. Li, L. Gu and R. Song, *Appl. Catal. B: Environ.*, 2023, **325**, 122354.

[26] R. Guo, Y. Zhang, X. Zhang, H. Yang and T. Hu, *Chem. Eng. J.*, 2024, **491**, 152028.

[27] K. Wu, C. Wang, X. Lang, J. Cheng, H. Wu, C. Lyu, W.-M. Lau, Z. Liang, X. Zhu and J. Zheng, *J. Colloid Interface Sci.*, 2024, **654**, 1040–1053.

[28] L. Zhang, M. Li, C. Sun, H.-T. Wang, Y. Xiao, K. Ma, Y. Cai, C.-Y. Lee, Y.-C. Shao, C.-H. Wang and S. Zhao, *Adv. Funct. Mater.*, 2025, **35**, 2420163.

[29] R. Govindasamy, C. J. Moon, R. A. Senthil, V. Maheskumar, A. Kumar, S. Lee, M. Ubaidullah and M. Y. Choi, *Chem. Eng. J*, 2025, **522**, 167074.

[30] D. Qu, S. Zeng, Z. Yang, J. Wang, Y. Zheng, J. Pan, J. Cao and C. Li, *ACS Appl. Nano Mater.*, 2024, **7**, 28669–28679.

[31] X. Ren, and Y. Tong, *Int. J. Hydrogen Energy*, 2024, **49**, 489–497.